J. Fluid Mech. (2006), *vol.* 548, *pp.* 141–150. © 2006 Cambridge University Press
doi:10.1017/S0022112005007718 Printed in the United Kingdom

Capillary rise between elastic sheets

By HO-YOUNG KIM[1] AND L. MAHADEVAN[2]†

[1]School of Mechanical and Aerospace Engineering, Seoul National University, Seoul 151-744, Korea

[2]Division of Engineering and Applied Sciences, Harvard University, Cambridge, MA 02138, USA

(Received 15 August 2005 and in revised form 23 October 2005)

When a paintbrush is dipped into a pot of paint and pulled out, surface tension forces cause the individual hairs in the brush to coalesce even as the brush becomes impregnated with paint. We study a simple model of this elastocapillary interaction in the context of the surface-tension-driven vertical rise of a liquid between two long flexible hydrophilic sheets that are held a small distance apart at one end. We provide an analytic theory for the static shapes of the sheets as well as the liquid rise height which is different from that of the classical law of Jurin, and show that our experiments are quantitatively consistent with the theory.

1. Introduction

The hairs or bristles of a paint brush come together when the brush is removed from the liquid. The reason for this is simple: surface tension forces at the air–water–hair interface tend to minimize the energy of the system, here consisting of the elastic energy of the deformed hairs, gravity and the capillary energy of the liquid–vapour interface. For a given type of paint, the pointedness of the tip of the brush, a parameter that determines the width of a paint stroke, is thus a function of the relative stiffness of the bristles, which in turn depends on their length, their areal density at the clamp and the material of which they are made. This of course is why artists need a wide array of brushes to ply their art and play their part. The rise of liquid along and through the network of flexible hairs when the tip of the brush is just dipped in the liquid or when a fully immersed brush is taken out and allowed to drain under the influence of gravity determines the holding power of the brush and thus the length of a paint stroke. Understanding the fluid dynamics of painting requires that we characterize both the uptake to, and the spreading of paint from, the brush. Here we focus on a simple model that helps us understand the first process; the second is a variant of the Landau–Levich problem (Landau & Levich 1942), one we will not consider here.

Before we understand the uptake of paint by a soft brush, we revisit the simplest case of capillary rise, exemplified by the partial immersion of a vertical rigid narrow hollow capillary tube in a liquid. This leads to a rise or fall in the liquid level inside the tube relative to the ambient level because objects in partial contact with liquid and its vapour in the presence of a contact line experience interfacial forces at the three-phase junction. If the liquid has a contact angle that is less than a right angle, the liquid rises relative to its ambient level, while if the contact angle is greater than

† Author to whom correspondence should be addressed: lm@deas.harvard.edu

https://doi.org/10.1017/S0022112005007718 Published online by Cambridge University Press

a right angle, the liquid level falls. In either case, the rise/fall of the liquid stops when the hydrostatic pressure balances that due to surface tension, leading to the well-known law of Jurin (Jurin 1718). Thus, for a rigid wettable tube of radius r that is partially in a reservoir of liquid of density ρ and interfacial tension σ, the capillary rise length (or Jurin length) $l_J = 2\sigma/\rho g r$, where g is the acceleration due to gravity. For a capillary of radius $r \sim 100\,\mu\text{m}$ wetted by water, this leads to $l_J \sim 15\,\text{cm}$.

If the capillary tube is sufficiently flexible, Jurin's law is modified because of the ability of the interfacial forces to deform the tube. A variant of this problem has been well-studied as a model for how flexible capillaries or airways may collapse as a bubble moves through them (Grotberg & Jensen 2004). In this regime, tension in the tube dominates the elastic response to hydrodynamic forces as fluid mensicus moves through it. However, if the tube is replaced by flexible sheets or hairs with free ends as in a paint brush, the dominant elastic contribution is due to sheet or hair bending. Here we focus on this qualitatively different bending-dominated regime and consider a simple model brush: two flexible sheets of length L clamped at a distance w apart, and free at the other end. When this system is dipped in a liquid, capillary forces associated with the high curvature of the mensicus between the sheets lead to a negative pressure that causes the liquid to rise between the sheets. Simultaneously, the sheets come together under the influence of this same negative pressure. For short and stiff sheets, the liquid rise is assisted by a slight decrease in the gap between the sheets, suggesting but a perturbative correction to the law of Jurin. However, when the sheets are long and flexible, they are nearly stuck together at the free ends with almost no liquid in between, showing a qualitatively different behaviour from the Jurin regime. After this work was underway, we became aware of similar work exploring this latter regime using a combination of experiments and scaling arguments (Bico *et al.* 2004). Our approach complements this by investigating all the regimes quantitatively from both a theoretical and experimental viewpoint.

We start with dimensional analysis. The scaled capillary rise height l_m/L must be a function of some dimensionless parameters. In addition to the aspect ratio of the system w/L, there are two other dimensionless length scales in the problem: the scaled capillary length l_c/L, where $l_c = (\sigma/\rho g)^{1/2}$, and a scaled adhesion or bending length l_a/L, where $l_a = (B/\sigma)^{1/2}$ (Cohen & Mahadevan 2003), B being the bending stiffness per unit width of the sheets. Thus, we may write $l_m/L = f(w/L, l_c/L, l_a/L)$. In addition, for partially wettable sheets, we expect a dependence on the contact angle at the solid–liquid–vapour boundary. When $l_a/L \to \infty$, corresponding to the case of rigid sheets, we recover Jurin's law $l_m \sim l_c^2/w$. When $l_a/l \sim O(1)$, we expect a small perturbation to this solution due to the small deflection δ of the sheet due to surface tension. Balancing the torque exerted on the sheet $B\delta/L^2$ with the capillary–gravity torque $\rho g l_J^2 L$ yields $\delta \sim w/\eta$, where $\eta = l_a^2 w^3/l_c^2 L^3$. Substituting the result in the equation for pressure balance at the meniscus $\sigma/(w-\delta) \sim \rho g l_m$ yields $l_m \sim l_J(1-k/\eta)^{-1}$, where $k = k(w/L)$. We see that when $\eta \gg 1$, the effects of capillary adhesion are dominated by sheet elasticity, so that the sheet deforms but slightly. However, when $\eta \ll 1$, the sheet bends easily due to capillary forces, resulting in the sticking of the sheets over much of their length, so that the quantity of interest is the dry length $l_d = x_m = L - l_m$. To understand this limit, we note that the sheet is deformed by an amount w over the dry length l_d. Minimizing the sum of the elastic energy of the deformed sheets Bw^2/x_m^3 and the interfacial energy $-\sigma(L-x_m)$ yields $l_d \sim (B/\sigma)^{1/4} w^{1/2} \sim (l_a w)^{1/2}$ (Bico *et al.* 2004). To go beyond these scaling estimates and understand the transitions between the different regimes, the quantitative dependence of the liquid rise height and shape of the sheets on the various dimensionless parameters, we formulate and solve a free boundary problem for these quantities.

https://doi.org/10.1017/S0022112005007718 Published online by Cambridge University Press

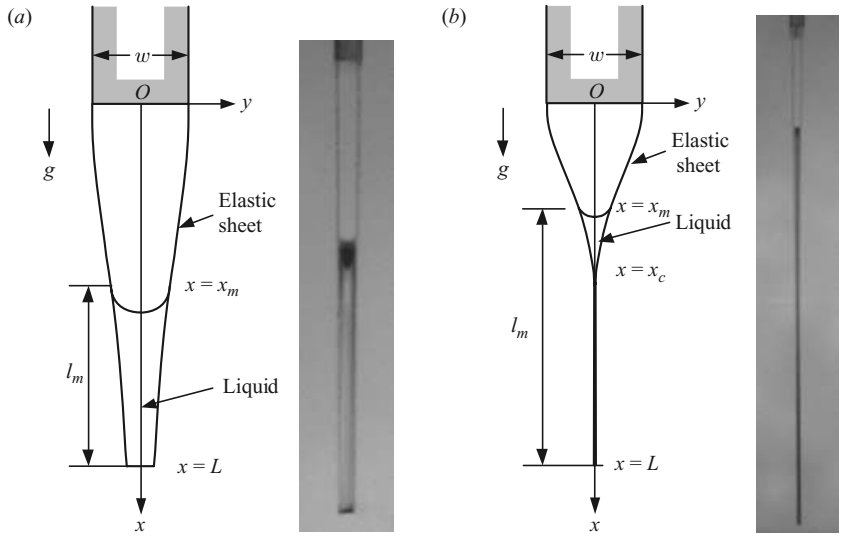


FIGURE 1. Schematic and shape of the sheets when (*a*) the sheets are relatively stiff so that the ends are separate: coordinate system and experimental image of glass cover slips, 24 mm long and initially 1 mm apart, after they were slowly withdrawn out of water; (*b*) the sheets are relatively soft so that ends are in contact: coordinate system and experimental image of glass sheets, 42 mm long and initially 0.6 mm apart, slowly withdrawn out of water.

2. The free boundary problem: formulation, solution and experimental corroboration

When the clamping distance $w \ll L$ the length of the sheets, the slope of the sheets $w/L \ll 1$, so that we may use a geometrically and physically linear theory of plates to describe their deformation. Symmetry of the configuration implies that we need to consider only one of the sheets – the other is simply a mirror image of the first about the vertical axis. Balance of forces in the direction transverse to the sheet then yields the general equation for the shape of the sheet $y(x)$ relative to the vertical (Landau & Lifshitz 1986)

$$By''''(x) = q(x). \tag{2.1}$$

Here x is the distance along the centreline of the sheets (which is effectively the same as the arclength coordinate for small deformations, as assumed here) measured from the clamped end, $y' \equiv \mathrm{d}y/\mathrm{d}x$, B is the flexural rigidity per unit width of the sheet and $q(x)$ is the force per unit area on the sheet.

2.1. *Capillary rise between stiff plates with separated ends*

In figure 1(*a*) corresponding to the case when $\eta \sim O(1)$, i.e. in the relatively stiff regime, we see that the sheets are in contact with liquid (water) over an unknown length $L - x_m$ and in contact with vapour (air) over a length x_m. Then, in the region for $0 < x < x_m$, where there is no hydrostatic pressure $q(x) = 0$, $y = y_1(x)$ satisfies

$$y_1'''' = 0, \quad 0 < x < x_m. \tag{2.2}$$

In the region $x_m < x < L$, there is a linearly varying hydrostatic pressure due to gravity with a boundary condition given by applying the Young–Laplace equation for the meniscus at the free end. This yields a transverse pressure on the sheet given by $q(x) = ax + b = \rho g(x - L) - \sigma\kappa_b$, where κ_b is the curvature of the mensicus at the

https://doi.org/10.1017/S0022112005007718 Published online by Cambridge University Press

bottom of the sheet, $x = L$. Then we see that the shape of the sheet in this region $y = y_2(x)$ satisfies

$$B y_2'''' = \rho g (x - L) - \sigma \kappa_b, \quad x_m < x < L. \tag{2.3}$$

Observations show that the curvature of the mensicus almost vanishes near the bottom of the sheet, a condition which we will use forthwith. Microscopically, the shape of the meniscus is determined by the details of the shape of the sheet edge and the contact angle of the interface; here we will ignore the correction due to this which is bound to be small since the dominant force balance involves hydrostatic pressures and elastic deformations over most of the sheet.

To complete the formulation of the problem, we need to specify some boundary and matching conditions that accompany (2.2)–(2.3) and determine the eight constants of integration and the unknown meniscus height $l_m = (L - x_m)$. The sheet is clamped vertically at the end $x = 0$ so that the corresponding boundary conditions are $y_1(0) = w/2$ and $y_1'(0) = 0$. At the other end, $x = L$, the sheet is free of torques, but is subject to a transverse shear force due to surface tension. Therefore, we may write: $y_2''(L) = 0$ and $B y_2'''(L) = \sigma \sin\theta_b$, where θ_b is the contact angle at $x = L$. Our experimental observations suggest that $\theta_b \approx 90^\circ$, so that $y_2'''(L) = \sigma/B$. These four boundary conditions must be supplemented by matching conditions at the meniscus $x = x_m$ given by the continuity of the deflection, the slope, and the curvature of the sheet, i.e. $y_1(x_m) = y_2(x_m)$, $y_1'(x_m) = y_2'(x_m)$ and $y_1''(x_m) = y_2''(x_m)$. Furthermore, the transverse shear force suffers a jump across $x = x_m$ due to the surface tension which acts along the contact line and yields: $B y_1'''(x_m) - B y_2'''(x_m) = \sigma \sin\theta_t$. Here θ_t is the contact angle at the free mensicus $x = x_m$, and vanishes for the case of perfectly wetting surfaces. This last jump condition follows directly by integrating (2.2)–(2.3) across an infinitesimal section that includes the meniscus. Finally, there is a pressure jump across the meniscus so that $\rho g (L - x_m) = \sigma \cos\theta_t / y_1|_{x = x_m}$.

Next, we scale the equations and boundary conditions to make them dimensionless. We use L to scale the coordinate along the length of the sheet x, and w to scale the sheet deflection $y(x)$, so that the complete boundary value problem may be written in dimensionless form as

$$\tilde{y}_1'''' = 0, \quad 0 < \tilde{x} < \tilde{x}_m, \tag{2.4}$$

$$\tilde{y}_2'''' = \frac{L^5}{l_c^2 l_a^2 w} (\tilde{x} - 1), \quad \tilde{x}_m < \tilde{x} < 1, \tag{2.5}$$

subject to the conditions

$$\left.\begin{aligned}
\tilde{y}_1|_{\tilde{x}=0} &= 1/2, & \tilde{y}_1'|_{\tilde{x}=0} &= 0, \\
\tilde{y}_2''|_{\tilde{x}=1} &= 0, & \tilde{y}_2'''|_{\tilde{x}=1} &= L^3/w l_a^2, \\
\tilde{y}_1|_{\tilde{x}=x_m} &= \tilde{y}_2|_{\tilde{x}=x_m}, & \tilde{y}_1'|_{\tilde{x}=x_m} &= \tilde{y}_2'|_{\tilde{x}=x_m}, \\
\tilde{y}_1''|_{\tilde{x}=x_m} &= \tilde{y}_2''|_{\tilde{x}=x_m}, & (\tilde{y}_1''' - \tilde{y}_2''')|_{\tilde{x}=x_m} &= L^3 \sin\theta_t / w l_a^2, \\
\cos\theta_t / \tilde{y}|_{\tilde{x}=\tilde{x}_m} &= w l_m / l_c^2. & &
\end{aligned}\right\} \tag{2.6}$$

Integrating (2.4)–(2.5) yields a simple cubic polynomial solution for $\tilde{y}_1$ and a quintic polynomial $\tilde{y}_2$, with a total of eight integration constants and the unknown meniscus $\tilde{x}_m$. These unknowns are obtained by substituting the solutions into the nine boundary conditions (2.6), and solving the resulting algebraic system to yield closed-form expressions for $\tilde{y}_1(x)$ and $\tilde{y}_2(x)$.

To visualize these solutions, in figure 2 we show the dimensionless shape of one of the sheets $y(x)/w$ as a function of the naturally appearing dimensionless parameters

https://doi.org/10.1017/S0022112005007718 Published online by Cambridge University Press

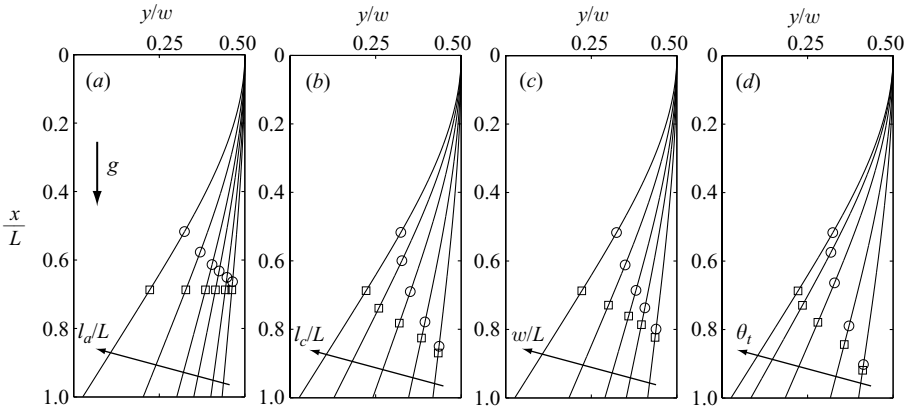


FIGURE 2. Effects of dimensionless parameters on the scaled sheet shape and the location of the upper meniscus x_m (circles) obtained by solving (2.4)–(2.6). The sheets are dry from $x/L = 0$ down to the circles. The squares denote the height of liquid assuming rigid sheets. For purposes of comparison, the leftmost curve in each case corresponds to the parameter values $l_a/L = 15.4$, $l_c/L = 0.0751$, $w/L = 0.0361$, and $\theta_t = 0$, corresponding to the following parameter values for water rising between two thin sheets of length $L = 36$ mm separated by a nominal distance $w = 1.3$ mm, and $B = 0.022$ Nm, $\sigma = 0.072$ N m^{-1}, $\rho g = 9800$ N m^{-3}. (*a*) l_a/L decreases in the direction of the arrow taking the values 32.8, 27.4, 23.2, 20.7, 18.0, and 15.4. (*b*) l_c/L increases in the direction of the arrow taking the values 0.0486, 0.0561, 0.0627, 0.0687, and 0.0751. (*c*) w/L decreases in the direction of the arrow taking the values 0.0639, 0.0528, 0.0472, 0.0417, and 0.0361. (*d*) θ_t decreases in the direction of the arrow taking the values 75°, 60°, 45°, 30°, and 0°.

in the problem: l_a/L, l_c/L, w/L, and θ_t. In each case, we show the location of the meniscus, and for comparison, the location of the mensicus for a set of rigid sheets for which $l_m = L - x_m = l_J = 2\sigma/\rho g w$, the Jurin length. The trends are intuitively obvious; the capillary rise length l_m is not much more than the Jurin length for stiff sheets or those that have a low interfacial tension, but can be as much as twice the Jurin length for soft sheets in contact with a liquid with a large interfacial tension. In terms of the parameter $\eta = l_a^2 w^3/l_c^2 L^3$ the leftmost sheet in each of the panels in figure 2 corresponds to $\eta \approx 2$, where the sheet ends are still separated. As η decreases further, the sheets becomes relatively more flexible leading to contact between the sheets and changing the problem qualitatively. Before treating this case, we now turn to a comparison of the theory of capillary rise between stiff elastic sheets with experiments.

Experimentally, there are two paths to the equilibrium shape of the sheets and the meniscus height. In one case, the sheets are completely wetted by water by immersion and then withdrawn slowly so that the receding meniscus may find its equilibrium (wet-to-dry method). In the other case, the free edges of the sheets which are in air are brought into contact with the air–water interface causing water to rise up rapidly in the narrow gap, eventually slowing down and stopping when the meniscus reaches its equilibrium (dry-to-wet method). It turns out that these two approaches lead to almost identical values of the equilibrium meniscus rise, although their dynamics are very different, a fact that we will discuss later. The glass sheets were cleaned with piranha solution (Senturia 2001) that makes them almost perfectly wettable by water ($\theta_t \approx 0$) with negligible contact angle hysteresis. When the sheets are shorter than the Jurin length, l_J, the entire sheets are wetted. In this case, the sheet shape can be obtained by solving (2.5) for $0 < x < L \leqslant l_J$ with the first four boundary conditions

https://doi.org/10.1017/S0022112005007718 Published online by Cambridge University Press

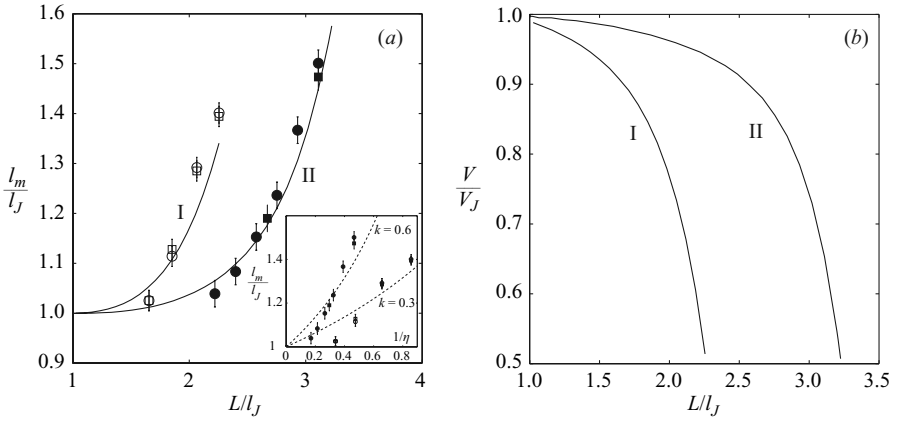


FIGURE 3. (*a*) Comparison of experimental results and theoretically predicted capillary rise height l_m (solid lines) obtained by solving (2.4)–(2.6). Inset: Replotting the experimental results and the scaling law $l_m/l_J \sim (1 - k/\eta)^{-1}$ with adjustable k also shows reasonable agreement. Line I and open symbols are for $w/l_c = 0.37$. Line II and filled symbols are for $w/l_c = 0.48$. The circles and squares correspond to the results of the wet-to-dry and the dry-to-wet methods, respectively. (*b*) Trapped water volume versus the length of the sheet with $B = 0.022$ Nm based on the sheet shapes obtained by solving (2.4)–(2.6). The volume is scaled by the trapped volume between rigid sheets. The trapping efficiency, V/V_J, decreases with the increase of the sheet length. Lines I and II correspond to $w/l_c = 0.37$ and $w/l_c = 0.48$, respectively.

in (2.6) due to the absence of the top meniscus. The equilibrium solution is readily obtained as $y = (ax^5 + bx^4 + cx^3 + dx^2 + Bw/2)/B$ where $a = \rho g/120$, $b = -\rho gL/24$, $c = (\sigma + \rho gL^2/2)/6$, and $d = -(\rho gL^3/6 + \sigma L)/24$ in dimensional form. The effects of the dimensionless parameters such as l_a/L, l_c/L, and w/L on the sheet shape are similar to those shown in figure 2. Figure 3(*a*) shows that for sheets longer than l_J, both the wet-to-dry (filling) and the dry-to-wet (draining) experiments result in capillary rises, $l_m = L - x_m$, that are larger than l_J because the gap narrows due to negative relative pressure in the trapped liquid. For comparison we plot the scaled capillary rise length l_m/l_J obtained by solving (2.4)–(2.6) as a function of the parameter L/l_J for two values of separation w. We see that the theory compares well with experiments. In the inset of figure 3(*a*), we show the comparison with the scaling introduced in the introduction $l_m \sim l_J(1 - k/\eta)^{-1}$ that also is reasonably good for small $1/\eta$.

Knowing the sheet shape allows us to calculate the capillary lifting capacity of the sheets. In figure 3(*b*), we show that the scaled volume of the liquid trapped between elastic sheets V/V_J, where $V_J = l_J w$, is always less than unity. This follows from the fact that for a given interfacial tension, the condition at the meniscus sets the pressure drop across it. This drop is larger for softer sheets, pulling them further in. Since the pressure increases linearly with depth while the shape of the sheet does not, the volume enclosed is smaller. An obvious conclusion is that with all other things being equal, a softer paint brush also has a shorter stroke, consistent with our intuition and experience.

2.2. *Capillary rise between soft sheets with contacting ends*

If the sheets are relatively soft, i.e. $\eta \ll 1$, which effect may be brought about by increasing their length or decreasing their flexural rigidity, surface tension causes the sheets to completely close at the free end as shown in figure 1(*b*). The formulation

https://doi.org/10.1017/S0022112005007718 Published online by Cambridge University Press

of the resulting free boundary problem changes slightly now, since there are two unknown locations: the wet–dry meniscus x_m, and the location of the contact line x_c beyond which the sheets are effectively in contact. The transition to this regime from the case when the sheet ends are separated is most naturally thought of in terms of a continuously increasing change in the length of the sheets. As the sheets become longer and longer, the separation between them at $x = L$ becomes smaller and eventually vanishes when the sheet length is say L_1. A further increase in $L > L_1$ causes the angle between the sheets at their contacting ends, still at $x = L$, to decrease until eventually it too vanishes when the sheet length is say $L = L_2$, leading to smooth tangential contact between the sheets along a line. Still further increase in the length of the sheets, with $L > L_2$, then causes the contact line between the sheets to move to an unknown location $x = x_c$. Thus, the formulation of the free boundary problem changes slightly for each of these regimes. When $L_1 < L < L_2$, the governing equations are still (2.4)–(2.5) but the boundary condition $\tilde{y}_2'''|_{\tilde{x}=1} = L^3/wl_a^2$ is replaced by $\tilde{y}_2|_{\tilde{x}=1} = 0$.

When $L > L_2$, the quantity of interest is no longer the capillary rise but the size of the dry and wet regions, as shown in figure 1(*b*). In the dry region, $0 < x < x_m$, the shape of the sheet still satisfies (2.2). In the wet region where the sheets are still apart, $x_m < x < x_c$, the governing equation (2.3) is modified slightly to account for the fact that at equilibrium the pressure at $x = x_c$ vanishes. Then, we may write

$$By_2'''' = \rho g(x - x_c), \quad x_m < x < x_c, \tag{2.7}$$

which condition ensures that we have a global force balance in the vertical direction (see the Appendix). The boundary conditions at $x = 0$ and the matching conditions at $x = x_m$ are identical to those for stiff sheets with separated ends. At $x = x_c$, where the sheets first touch each other, $y_2(x_c) = y_2'(x_c) = 0$ consistent with tangentially smooth contact. Furthermore, applying the principle of virtual work to the contact line requires that $By_2''^2(x_c)/2 = \sigma_{ss} - \sigma_{sl}$ where $\sigma_{ss} - \sigma_{sl}$ is the difference in the interfacial energy per unit area associated with contact between the solid sheets and that between the solid and liquid. However, if we assume that there is a thin intercalating layer of liquid even in the region $x_c < x < L$ where the solid sheets are in nominal contact, this condition simplifies to $y_2'' = 0$. There is however a jump in the transverse shear force between the sheets at $x = x_c$, where the sheets attract each other. The three conditions at $x = x_c$ when combined with the matching conditions at $x = x_m$, and force equilibrium at the upper meniscus, $\rho g(x_c - x_m) = \sigma \cos\theta_t / y_1|_{x_m}$, are sufficient to solve the differential equations (2.2) and (2.7), giving the sheet shape $y_1(x)$, $y_2(x)$, and the two unknown locations x_m and x_c, and their dimensionless counterparts. Figure 4 shows the sheet shape as its length changes, showing representative sheet shapes in the three different regimes, i.e. the separated end $L < L_1$, the transition $L_1 < L < L_2$, and the contacting end $L \geqslant L_2$ along with the shapes that separate these regimes.

In figure 5, we plot the theoretically calculated scaled capillary rise height l_m/l_J as a function of the scaled sheet length L/l_J for different end separations w. The solid line corresponds to the case when the ends do not touch, i.e. when $L < L_1$. The dotted line corresponds to the case $L_1 < L < L_2$ when the sheets touch with a non-vanishing contact angle. For $L > L_2 = x_c$, the sheets are in contact when $x > x_c$, with $l_m = L - x_m$, and x_m being a constant, shown as another solid line. Over the entire range of sheet lengths, we find good agreement between theory and experiments performed using both the wet-to-dry and dry-to-wet methods, owing to negligible contact angle hysteresis. Although the capillary rise heights l_m/l_J are similar for different w/l_c, they do not collapse onto a master curve: this is because the smaller w/l_c is, the

https://doi.org/10.1017/S0022112005007718 Published online by Cambridge University Press

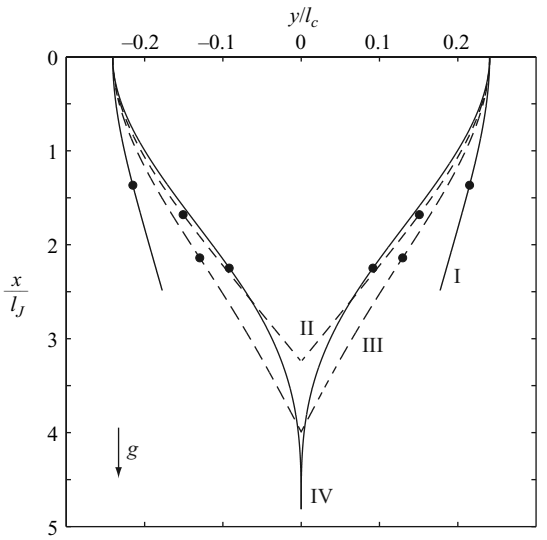


FIGURE 4. The theoretically predicted sheet shapes when $L < L_1$ (line I), $L = L_1$ (line II), $L_1 < L < L_2$ (line III), and $L = L_2$ (line IV) with the scaled distance between the sheets $w/l_c = 0.48$ at their clamped ends. As the sheet length increases from L_1 to L_2, the angle between the sheets gradually decreases until it reaches zero. The circles indicate the location of the upper meniscus of water.

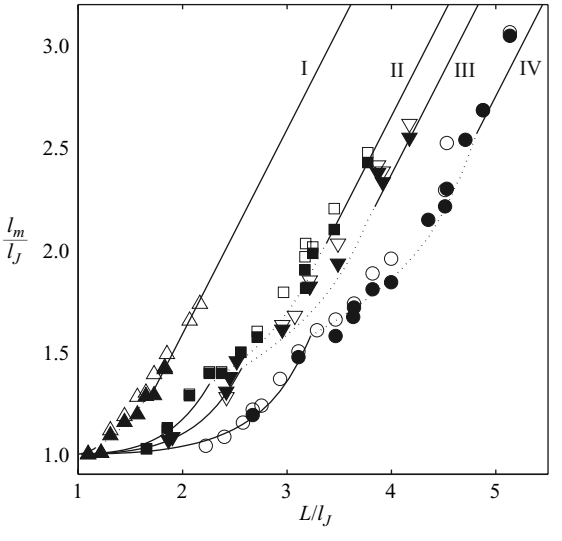
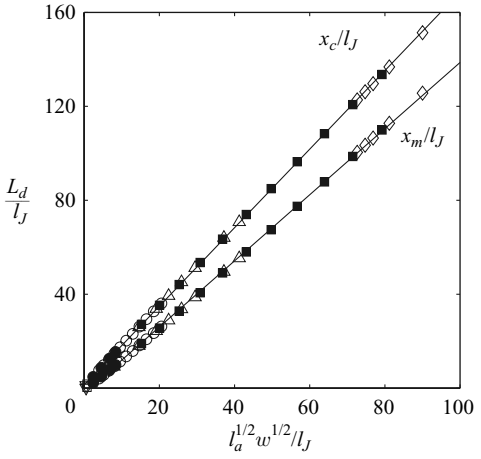


FIGURE 5. Theoretical and experimental results for entire length range. The regime changes from that for stiff plates with $l_J < L < L_1$ (solid line), to that for the transition $L_1 < L < L_2$ (dotted line), and finally to the case for soft sheets with $L > L_2$ (solid line) as L/l_J increases. Line I and the up triangles correspond to the theoretical and experimental results respectively with $w/l_c = 0.22$; line II and the squares correspond to the case with $w/l_c = 0.37$; line III and the down triangles correspond to the case with $w/l_c = 0.41$; line IV and the circles correspond to the case with $w/l_c = 0.48$. The open symbols are from the wet-to-dry method and the filled symbols the dry-to-wet method.

https://doi.org/10.1017/S0022112005007718 Published online by Cambridge University Press



	B (Nm)	σ (N m^{-1})
▽	0.0002	0.0717
□	0.001	0.0717
△	0.022	0.0200
●	0.022	0.0717
■	0.300	0.0200
◇	0.500	0.0200
○	0.800	0.0717

FIGURE 6. The computed locations of the scaled meniscus x_m/l_J and the contact lines x_c/l_J for various values of B, σ and w for the case when the sheets have contacting ends. Here w varies in the range between 0.5 and 3 mm. The solid line is the least-square fit based on the computed data points, consistent with a simple balance between elasticity and capillarity (see text).

more enhanced the scaled capillary rise height is. Furthermore the transition to the contacting sheet regime takes place later, i.e. for larger L/l_J as w/l_c increases.

Finally, we turn to the case when $L \gg L_2$. Here the quantities of interest are the location of the contact line x_c and the meniscus x_m. Solving (2.2) and (2.7) subject to the appropriate boundary conditions discussed above allows us to determine the values of x_m and x_c. Figure 6 shows that $x_m/l_J \approx 1.41\, l_a^{1/2}w^{1/2}/l_J$ and $x_c/l_J \approx 1.67\, l_a^{1/2}w^{1/2}/l_J$. This is consistent with the scaling/experimental results of Bico *et al.* (2004) which show that $l_d \approx 1.46(B/\sigma)^{1/4}w^{1/2}$, but our quantitative theory allow us to discriminate between the locations of the meniscus x_m and the contact line x_c.

3. Discussion

We have presented a simple theory for the capillary rise of a liquid in a narrow gap separating two flexible sheets, and corroborated the results using experiments. Our focus in this paper has been on the static equilibrium properties. One can quite reasonably ask how long it takes for the system to reach this equilibrium. The characteristic time for the meniscus to attain the equilibrium rise height is given by balancing the rate of work done against gravity by the capillary forces with the viscous dissipation rate. For rigid sheets separated by a distance w, this yields $\rho g w l_m(l_m/\tau) \sim \mu l_m w(l_m/\tau)^2/w^2$ so that $\tau \sim \mu l_m/\rho g w^2$. Our scaling analysis shows that when the sheet deformation is insignificant, the time it takes for the water meniscus to reach equilibrium is less than 1 s for $w \sim 1$ mm and $l_m \sim 10$ mm. However, as the sheet deforms significantly, the characteristic time to reach equilibrium increases rapidly, being limited by the narrowest region near the free ends. When L exceeds L_1, the bottom gap ϵ tends to close, so that the characteristic time reaches the order of 10 s for $\epsilon \sim 10\,\mu$m and 1000 s for $\epsilon \sim 1\,\mu$m. In our experimental study, we waited up to an hour for the water meniscus to reach equilibrium while maintaining the contact between the sheets and the water pool.

When fully immersed sheets are withdrawn from the liquid pool faster than the meniscus can reach its equilibrium, the dynamics of draining becomes an important

https://doi.org/10.1017/S0022112005007718 Published online by Cambridge University Press

parameter in determining the transient lifting capacity of the sheets. These transient effects become particularly important if the sheets are pulled out at a rate comparable to or faster than the characteristic speed of the meniscus in the beginning, $\rho g w^2/\mu$. This was qualitatively observed in the experiments performed through this work, although a detailed discussion of drainage requires that we consider the transient effects in elastocapillarity phenomena by modifying the theory of Hosoi & Mahadevan (2004) originally proposed for the elastohydrodynamics of thin sheets immersed in a fluid and moving close to a wall.

We thank the Schlumberger Chair Fund (L. M.) at Cambridge University for support that helped to initiate this work when we were there.

Appendix. Vertical force balance

The left–right symmetry of the system guarantees that globally horizontal forces and torques are automatically balanced. However, since gravity breaks up–down symmetry, we must check that globally vertical forces are also balanced. In the vertical direction, the liquid weight should be balanced by the sum of the vertical component of surface tension acting along the contact line of the upper meniscus and the reaction of the sheet in the wet region so that

$$\int_{x_m}^{x_c} \rho g y_2 \, \mathrm{d}x = \sigma \cos\theta_t - \int_{x_m}^{x_c} B y_2'''' y_2' \, \mathrm{d}x, \tag{A 1}$$

where x_c can be replaced by L in the case of the separated-end configuration. The negative sign in front of the second term on the right-hand side means that the sheet pulls the liquid downward in reaction to the hydrostatic force that pulls the sheet upward.

Here we show that the vertical force balance is automatically satisfied by combining (2.7) with the boundary condition at the upper meniscus. Multiplying (2.7) by y_2' and integrating over the domain, we get

$$\int_{x_m}^{x_c} B y_2'''' y_2' \, \mathrm{d}x = \int_{x_m}^{x_c} \rho g (x - x_c) y_2' \, \mathrm{d}x. \tag{A 2}$$

Integrating the right-hand side by parts yields

$$\int_{x_m}^{x_c} B y_2'''' y_2' \, \mathrm{d}x = \rho g (x_c - x_m) y_2|_{x_m} - \int_{x_m}^{x_c} \rho g y_2 \, \mathrm{d}x. \tag{A 3}$$

Finally, pressure balance at the upper meniscus gives $\rho g (x_c - x_m) y_2|_{x_m} = \sigma \cos\theta_t$. Therefore, (A 3) is identical to (A 1).

REFERENCES

Bico, J., Roman, B., Moulin, L. & Boudaoud, A. 2004 *Nature* **432**, 690.
Cohen, A. E. & Mahadevan, L. 2003 *Proc. Natl Acad. Sci.* **100**, 12141–12146.
Grotberg, J. B. & Jensen, O. E. 2004 *Annu. Rev. Fluid Mech.* **36**, 121–147.
Hosoi, A. E. & Mahadevan, L. 2004 *Phys. Rev. Lett.* **93**, 137802.
Jurin, J. 1718 *Phil. Trans.* **30**, 739–747.
Landau, L. D. & Levich, B. 1942 *Acta Physicochim. URSS* **17**, 42–54.
Landau, L. D. & Lifshitz, E. M. 1986 *Theory of Elasticity*, 3rd Edn. Pergamon.
Senturia, S. D. 2001 *Microsystem Design*. Kluwer.

https://doi.org/10.1017/S0022112005007718 Published online by Cambridge University Press